DENTAL MATERIALS 35 (2019) 1665–1681

Available online at www.sciencedirect.com

ScienceDirect

journal homepage: www.intl.elsevierhealth.com/journals/dema

Novel nanotechnology and near-infrared photodynamic therapy to kill periodontitis-related biofilm pathogens and protect the periodontium

Manlin Qi[a], *Xue Li*[a], *Xiaolin Sun*[a], *Chunyan Li*[a], *Franklin R. Tay*[b], *Michael D. Weir*[c], *Biao Dong*[d,*], *Yanmin Zhou*[a,*], *Lin Wang*[a,*], *Hockin H.K. Xu*[c,e,f]

[a] *Department of Oral Implantology, School and Hospital of Stomatology, Jilin University, Changchun, 130021, China*
[b] *The Dental College of Georgia, Augusta University, Augusta, GA, USA*
[c] *Department of Advanced Oral Sciences and Therapeutics, University of Maryland School of Dentistry, Baltimore, MD 21201, USA*
[d] *State Key Laboratory on Integrated Optoelectronics, College of Electronic Science and Engineering, Jilin University, Changchun 130012, China*
[e] *Center for Stem Cell Biology & Regenerative Medicine, University of Maryland School of Medicine, Baltimore, MD 21201, USA*
[f] *Marlene and Stewart Greenebaum Cancer Center, University of Maryland School of Medicine, Baltimore, MD 21201, USA*

ARTICLE INFO

Keywords:
Titanium dioxide
Upconversion nanoparticles
Antibacterial
Near-infrared
Photodynamic therapy
Periodontitis biofilms

ABSTRACT

Objective. Periodontal tissue destruction and tooth loss are increasingly a worldwide problem as the population ages. Periodontitis is caused by bacterial infection and biofilm plaque buildup. Therefore, the objectives of this study were to: (1) develop a near-infrared light (NIR)-triggered core-shell nanostructure of upconversion nanoparticles and TiO_2 (UCNPs@TiO_2), and (2) investigate its inhibitory effects via antibacterial photodynamic therapy (aPDT) against periodontitis-related pathogens.

Methods. The core β-$NaYF_4$:Yb^{3+},Tm^{3+} were synthesized via thermal decomposition and further modified with the TiO_2 shell via a hydrothermal method. The core-shell structure and the upconversion fluorescence-induced aPDT treatment via 980 nm laser were studied. Three periodontitis-related pathogens *Streptococcus sanguinis* (*S. sanguinis*), *Porphyromonas gingivalis* (*P. gingivalis*) and *Fusobacterium nucleatum* (*F. nucleatum*) were investigated. The killing activity against planktonic bacteria was detected by a time-kill assay. Single species 4-day biofilms on dentin were tested by live/dead staining, colony-forming units (CFU), and metabolic activity.

Results. The hexagonal shaped UCNPs@TiO_2 had an average diameter of 39.7 nm. UCNPs@TiO_2 nanoparticles had positively charged (+12.4 mV) surface and were biocompatible and non-cytotoxic. Under the excitation of NIR light (980 nm), the core $NaYF_4$:Yb^{3+},Tm^{3+} UCNPs could emit intense ultraviolet (UV) light, which further triggered the aPDT function of the shell TiO_2 via energy transfer, thereby realizing the remarkable antibacterial effects against planktons and biofilms of periodontitis-associated pathogens. NIR-triggered

* *Corresponding authors.*
E-mail addresses: dongb@jlu.edu.cn (B. Dong), zhouym@jlu.edu.cn (Y. Zhou), wanglin1982@jlu.edu.cn (L. Wang).
https://doi.org/10.1016/j.dental.2019.08.115

UCNPs@TiO_2 achieved much greater reduction in biofilms than control ($p < 0.05$). Biofilm CFU was reduced by 3–4 orders of magnitude via NIR-triggered aPDT, which is significantly greater than that of negative control and commercial aPDT control groups. The killing efficacy of UCNPs@TiO_2-based aPDT against the three species was ranked to be: *S. sanguinis* < *F. nucleatum* = *P. gingivalis*. Metabolic activities of biofilms were also greatly reduced via NIR-triggered aPDT ($p < 0.05$).

Significance. Upconversion fluorescence-based aPDT achieved strong inhibiting effects against all three species of periodontitis-related pathogens. This novel nanotechnology demonstrated a high promise to inhibit periodontitis, with exciting potential to combat other oral infectious diseases such as deep endodontic infections.

1. Introduction

Periodontal tissue destruction and tooth loss are increasingly a worldwide problem as the population ages. Periodontitis is a chronic inflammatory process initiated by bacterial infection affecting the supporting tissues around the tooth, resulting in bone loss, tooth mobility or even tooth loss [1]. Approximately 10% of the world population suffered from severe periodontitis, while the number was 20.4% in Southern Latin America, in 2010 [2]. Considerable evidence has confirmed that plaque biofilm is the initiator of periodontitis, and subgingival plaque is implicated in damaging periodontal tissues [3,4]. Large amounts of bacteria could accumulate on subgingival tooth surfaces, where early microbial colonizers would offer attachment substrates for the later microbial colonizers during the plaque biofilm formation [5]. Therefore, there is a critical need to eliminate subgingival biofilms to treat periodontitis.

Mechanical debridement is considered as the main periodontal therapy [6]. However, as the periodontal probing depth increases, the clearance of subgingival plague by mechanical debridement becomes more difficult due to anatomical factors (e.g., deep invaginations, root furcation), instrument shape and clinical experience [7,8]. Furthermore, deeper probing may increase the risk of surgical trauma and postoperative complications (e.g. bacteremia) [9]. Therefore, mechanical debridement could not achieve major clinical improvements in cases of advanced diseases and deep periodontal pockets [6], where antibiotics could serve as an adjunctive treatment for periodontitis. However, the emergence of antibiotic-resistant strains and bacterial resistance has dramatically increased due to long-term utilization of antibiotics [10]. In a recent study, 74.2% of the patients with chronic periodontitis showed subgingival periodontal pathogens resistant to one or more of the test antibiotics [11]. In addition, 55%, 43.3%, 30.3%, and 26.5% of the patients with chronic periodontitis revealed one or more test species being resistant in vitro to doxycycline, amoxicillin, metronidazole, or clindamycin, respectively [11]. Furthermore, both systemic and local antibiotics as adjunctive treatments for periodontitis were reported to have more than ten types of adverse effects [10,12].

To meet these challenges, antimicrobial photodynamic therapy (aPDT) has been investigated as a promising therapy for eradicating pathogenic bacteria in periodontal and peri-implant diseases [13,14]. The aPDT consists of three components: photosensitizers (PSs), light, and oxygen. The PS is excited by a wavelength of light and then transforms from the ground state to a high-energy triplet state. The triplet state PSs have a longer lifespan, enabling the activated PS to generate reactive oxygen species (ROS), which can lead to irreversible oxidative damage against microorganisms [15]. The aPDT has the advantages of easy operation, wide applications, high efficiency and no obvious drug resistance [16]. The first photosensitive drug was approved for treating actinic keratoses in 1999 by the U. S. Food and Drug Administration (FDA) [17]. Commercial PSs such as methylene blue (MB) and Toluidine blue O (TBO) have been used in clinical treatments for periodontitis and peri-implantitis [13]. The effect of aPDT associated with non-surgical therapy for periodontal treatment was controversial. Early studies showed that adjunctive applications of a single episode of aPDT failed to achieve additional improvement [18]. Recently, however, multiple sessions of aPDT as an adjunct to surgical periodontal treatment were shown to significantly improve the clinical parameters at 90 days post-operation [19]. Moreover, according to recent scientific evidence-based information gathered by the American Academy of Periodontology (AAP), when compared with conventional periodontal therapy, aPDT may provide similar clinical improvements in probing depth and clinical attachment level in patients with moderate to severe periodontitis [20].

Recently, titanium oxide (TiO_2) has attracted interest due to features such as low toxicity, good biocompatibility and high stability in a physiological environment [21]. Upon ultraviolet (UV) irradiation, TiO_2 could generate reactive oxygen species (ROS) and exert potent bactericidal and sterilizing effects against oral pathogens [22,23]. In a recent study, TiO_2 nanoparticle-containing dental adhesives were investigated to combat oral bacterial biofilms [23]. TiO_2 significantly reduced *Porphyromonas gingivalis* (*P. gingivalis*) upon UV irradiation and exhibited a continuous photocatalytic effect even after the termination of the UV irradiation [24]. However, due to the wide band gap, TiO_2 photo-absorption was limited to the UV light spectrum which restricted tissue penetration and might cause DNA damage, skin cancer and other skin disorders [25].

Compared to the UV light, the near-infrared (NIR) light has a much larger tissue penetration depth and less damage to tis-

sues. If NIR light can be converted into UV light, it is expected to break through the excitation bottleneck problem of this type of TiO_2 PSs. Rare earth-doped upconversion nanoparticles (UCNPs) are currently the most representative light conversion materials via an anti-Stokes emission process, which can effectively convert NIR light into visible light and UV light [26]. Furthermore, these UCNPs have stable optical properties, such as narrow emission bands, long lifetime, and stable emission position. More importantly, the excitation light is mainly in the first window of biology (700–1100 nm), possessing not only high tissue penetration depth with less damage, but also no background noise generation, which is beneficial for fluorescence imaging [26]. Considering that periodontal infections are always located at deep pockets, furcation and surface irregularities areas, therefore, if NIR triggered aPDT can be involved with deeper tissue penetration, it may become an important way to solve the current bottleneck problem, which is also of utmost importance for clinical therapeutic applications in periodontitis.

The present study synthesized a core-shell structured β-$NaYF_4$:Yb^{3+},Tm^{3+}@TiO_2 (termed UCNPs@TiO_2) for the first time. As shown in Scheme 1, the UCNPs core upconverts NIR light to UV light, which further photoexcites the electrons in the valence band (VB) of the TiO_2 shell to the conduction band (CB). This results in the formation of electron-hole pair and then eliciting redox reactions for the generation of ROS. This design could simultaneously take advantage of the deep penetration of NIR and the excellent photoelectron – catalysis performance of TiO_2 to produce ROS effectively. The aims of this study were to: (1) develop a novel core-shell structured UCNPs@TiO_2, and (2) investigate the antibacterial capabilities against periodontitis-associated pathogens for the first time. It was hypothesized that: (1) UCNPs@TiO_2 would have uniform size distribution without cytotoxicity; (2) UCNPs@TiO_2 would possess an excellent antibacterial activity against both planktons and biofilms of periodontitis-associated pathogens with the activation of NIR; (3) UCNPs@TiO_2 would be more effective against Gram-negative bacteria than Gram-positive bacteria.

2. Materials and methods

2.1. Materials and reagents

YCl_3, $YbCl_3$ and $TmCl_3$ (Ruike Centre, Baotou, China), Octadecene (ODE), oleic acid (OA), polyvinylpyrrolidone (PVP, Mw = 58,000, K29-32), and 1,3-diphenylisobenzo-furan (DPBF) were purchased from Aladdin, China. Other chemical reagents were purchased from Beijing Chemical Works, China. Dulbecco's Modified Eagle Medium (DMEM) and fetal bovine serum (FBS) was commercially obtained from Gibco (Grand Island, NY, USA). Cell Counting Kit-8 (CCK-8), paraformaldehyde, fluorescein isothiocyanate (FITC) and 4′, 6-diamidino-2-phenylindole (DAPI) were purchased from Sigma-Aldrich (St. Louis, MO, USA). All the bacteria strains obtained from American Type Culture Collection (ATCC, Manassas, VA): *Streptococcus sanguinis* (*S. sanguinis*) ATCC 49295, *P. gingivalis* ATCC 33277 and *Fusobacterium nucleatum* (*F. nucleatum*) ATCC 25586. Tryptic soy broth (TSB), menadione, yeast extract, L-cysteine hydrochloride, hemin, 3-[4,5-dimethylthiazol-2-yl]-2,5 diphenyl tetrazolium bromide (MTT) and dimethyl sulfoxide (DMSO) were purchased from Sigma-Aldrich (St. Louis, MO, USA). Columbia blood agar was purchased from BIO-KONT (Wenzhou, China). LIVE/DEAD BacLight Bacterial Viability Kits was obtained from Invitrogen (Carlsbad, CA, USA). All reagents were used without additional purification.

2.2. Synthesis of β-$NaYF_4$: Yb^{3+},Tm^{3+} UCNPs

The upconversion nanoparticle (UCNPs, β-$NaYF_4$:Yb^{3+},Tm^{3+}) core was synthesized as described previously with slight modifications [27]. Briefly, 0.795 mmol of YCl_3, 0.2 mmol of $YbCl_3$ and 0.005 mmol of $TmCl_3$ were mixed with 6 mL of OA and 15 mL of ODE in a 100 mL flask and heated to 160 °C to form a homogeneous solution for 1 h [27]. After cooling down to room temperature, 10 mL of methanol solution containing 2.5 mmol of NaOH and 4 mmol of NH_4F was slowly added dropwise into the flask and stirred over 30 min until a transparent solution was formed. The solution was subsequently heated to remove the methanol, degassed at 125 °C for 30 min, then heated to 330 °C and maintained under Argon protection for 1 h. When the solution was cooled to 60 °C, nanocrystals were precipitated with ethanol. This was washed three times with cyclohexane/ethanol at a volume ratio of 1:2. The final products were collected and re-dispersed in cyclohexane [27].

2.3. Coating of TiO_2 on β-$NaYF_4$:Yb^{3+},Tm^{3+} UCNPs

The coating process was according to the previous protocols with slight modifications [28]. The β-$NaYF_4$:Yb^{3+},Tm^{3+} UCNPs of 0.05 mmol were dispersed in 15 mL ethanol and mixed with 0.1 g PVP and 0.1 mL deionized water under magnetic stirring for 1 h to ensure sufficient adsorption of PVP. Then 0.02 mL tetrabutyl titanate was dissolved in 5 mL of ethanol which was added dropwise to the above suspension with continuous stirring for 2 h. Another 15 mL of ethanol was added into the aforementioned reaction solution. The solution was transferred into a 50 mL sealed Teflon-lined autoclave and maintained at 180 °C for 6 h. After the autoclave was cooled to room temperature, the precipitates were separated by centrifugation and washed three times with ethanol and deionized water [28]. The final products were dispersed in ethanol and referred as to UCNPs@TiO_2.

2.4. Characterization of the synthesized nanoparticles

The nanoparticles were examined using a transmission electron microscope (TEM, JEOL, JEM-2100 F, Japan) at an acceleration voltage of 200 kV. The purity and phase structure of the samples were characterized by X-ray power diffraction (XRD) with a RigakuD/max-rA power diffractometer (Rigaku, Tokyo, Japan) using a Cu-KR radiation (λ = 1.54178 Å) in the 2θ range from 10° to 80°. The Zeta potential of UCNPs@TiO_2 was measured using Zeta potential instrument (Malvern Instruments Limited, Zetasizer Nano-Z, UK). A spectrometer (Andor, Shamrock SR-750) was used to measure upconversion luminescent (UCL) spectra. The signal was collected by a photomultiplier combined with a monochromator from 300 nm to 800 nm. A continuous 980 nm diode laser was used to pump the samples for a steady-state spectra investigation. In the measurements

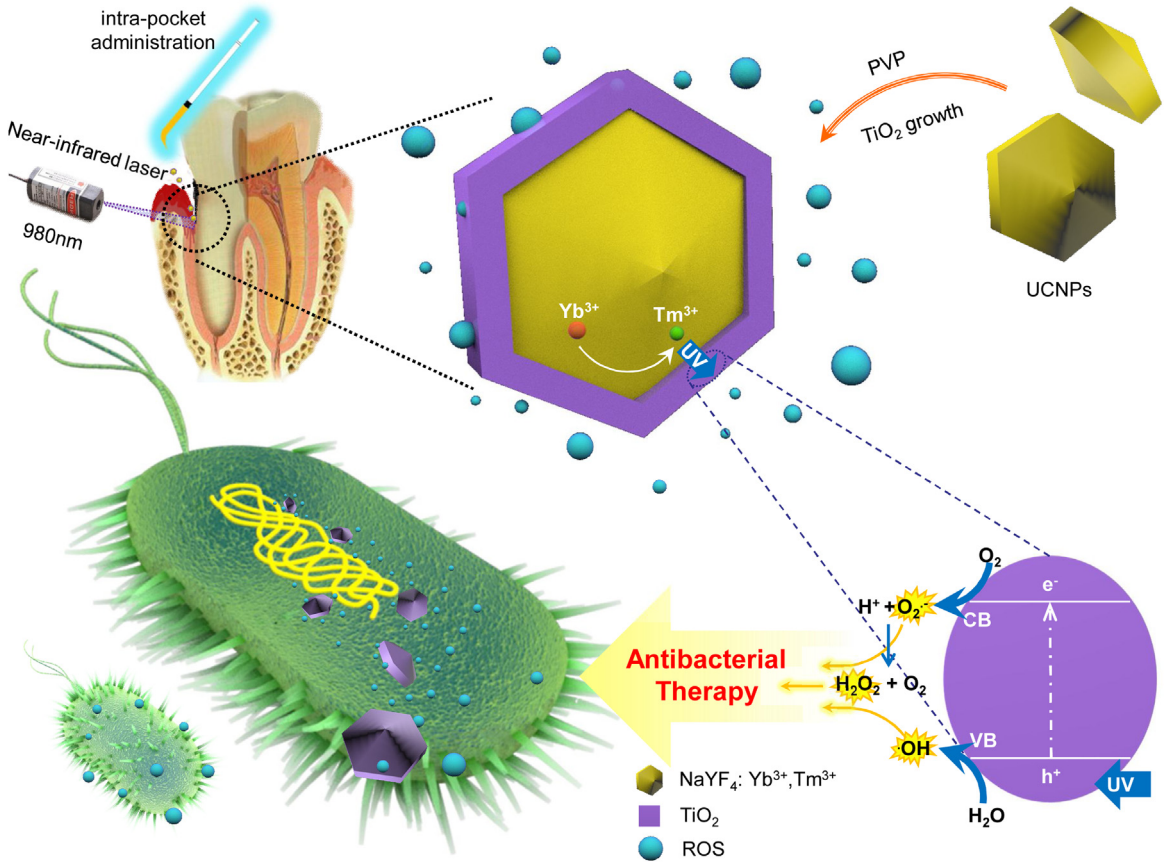

Scheme 1 – Synthesis of β-$NaYF_4$:Yb^{3+},Tm^{3+}@TiO_2 and mechanism of aPDT under NIR irradiation. Upon NIR irradiation, the UCNPs core upconverts NIR light to UV light, which further photoexcites the electrons in the valence band (VB) of TiO_2 shell to conduction band (CB). This results in the formation of electron-hole pair which migrate to the surfaces to generate various ROS containing superoxide radical ($O_2^{\bullet -}$), hydroxyl radical ($^{\bullet}OH$) and hydrogen peroxide (H_2O_2). ROS eventually causes oxidative damage against the microorganisms.

of luminescent dynamics, a laser-system including a Nd: YAG pumping laser (1064 nm), the third-order Harmonic-Generator (355 nm) and a tunable optical parameter oscillator (OPO, Continuum Precision II 8000) was applied to pump the samples. The following parameters were used: a pulse duration of 10 ns, a repetition frequency of 10 Hz, and a line width of 4–7 cm^{-1}. Ultraviolet-visible (UV–vis) absorption spectra were measured with a scanning spectrophotometer (Shimadzu, UV-3600PC UV–vis, Japan) ranging of 200–1100 nm.

2.5. *In vitro ROS production generation*

DPBF probes can react irreversibly with ROS to detect the generation of ROS quantum yield of UCNPs@TiO_2. The DPBF absorption was at 410 nm and the intensity decreased after reaction with ROS [29]. 10 mg of UCNPs@TiO_2 nanoparticles were well-dispersed in 2 mL of DPBF solution (0.5 mg/mL), and then diluted by 50 times. 2 mL of the mixture was transferred to a dark vessel with ultrasonic processing for 20 min. Then, the mixture was continuously irradiated by an optical probe with exposure to a 980 nm diode laser system (BWT Beijing Ltd., DS3-11313-0411, max: 5 W, 10,000 Hz, 45 μs) at a power density of 2.5 W cm^{-2} for up to 20 min. The absorption was measured at every 5 min of the irradiation [30]. The generation of ROS was determined by the characteristic absorption decrease of the DPBF using a UV–vis absorption spectrum.

2.6. *In vitro dark-toxicity measurement of UCNPs@TiO_2*

Mouse fibroblasts L929 cells (Shanghai Institute of Biochemistry and Cell Biology, China) were seeded at a density of 6×10^3 per well in a 96-well plate and incubated overnight to allow the cells to adhere to the bottom of the wells. The UCNPs@TiO_2 was prepared at a concentration ranged from 10 μM (2.7 μg/mL) to 4 mM (1.08 mg/mL) and then sonicated for 20 min in DMEM supplemented with 1% antibiotics (100 U/mL penicillin and 100 g/mL streptomycin) and 10% FBS. Cells were further incubated for 24 h at 37 °C, and then the number of viable cells was determined by CCK-8 assay using a microplate reader at OD_{450nm} (Bio-Tek, Winooski, VT, USA).

The morphology of L929 cells was observed following the above process by treatment with nanoparticles at a series of concentrations. Paraformaldehyde (4%) was used to fix the cells. Samples were washed with PBS. Subsequently, 10 μg/mL FITC and 1 μg/mL DAPI were added to stain the cells for 15 min.

The cell morphology was examined using a confocal laser scanning microscopy (CLSM, Olympus FV1000, Japan).

2.7. Bacteria strains and culture

The bacterial strains were *S. sanguinis*, *P. gingivalis* and *F. nucleatum*. Each species was incubated in TSB supplemented with yeast extract 5 g/L, L-cysteine hydrochloride 0.5 g/L, hemin 5 mg/L and menadione 1 mg/L at 37 °C under anaerobic environment (85% N_2, 10% H_2 and 5% CO_2) [31]. The inoculum was adjusted to 10^8 colony-forming unit counts (CFU/mL), based on the standard curve of OD_{600nm} versus CFU/mL for each species [31]. The inoculum was then diluted in the growth medium at a ratio of 1:10 and used for subsequent experiments.

2.8. Time-kill curves of UCNPs@TiO_2 against planktonic bacteria

The concentration of UCNPs@TiO_2 was set following the cell-toxicity measurement. Since significant cytotoxicity was detected at a concentration of 4 mM, whereas 2 mM was relative safe, concentrations of 1 mM and 2 mM were used in subsequent experiments. Accordingly, the following five groups were tested for antibacterial effects:

(1) (1) **Negative control group**: The bacteria were not treated with nanoparticles or laser irradiation (referred to as "Dark control");
(2) **Low dose UCNPs@TiO_2control group**: The bacteria were treated with 1 mM UCNPs@TiO_2 but without laser irradiation (referred to as "Dark+1 mM UCNPs@TiO_2");
(3) **High dose UCNPs@TiO_2control group:** The bacteria were treated with 2 mM UCNPs@TiO_2 but without laser irradiation (referred to as "Dark+2 mM UCNPs@TiO_2");
(4) **Low dose UCNPs@TiO_2aPDT group:** The bacteria were treated with 1 mM UCNPs@TiO_2 and with laser irradiation at 750 J cm^{-2} (referred to as "Light+1 mM UCNPs@TiO_2");
(5) **High dose UCNPs@TiO_2aPDT group:** The bacteria were treated with 2 mM UCNPs@TiO_2 and with laser irradiation at 750 J cm^{-2} (referred to as "Light+2 mM UCNPs@TiO_2").

For group (4) and (5), each well was irradiated with the 980 nm laser at a power of 2.5 W cm^{-2} for 5 min. The height of the laser head was adjusted to allow the laser spot to have the same size as the well size.

The killing activity of UCNPs@TiO_2 against planktonic bacteria (*S. sanguinis*, *P. gingivalis* and *F. nucleatum*) were detected via the time-kill curves. Briefly, *S. sanguinis*, *P. gingivalis*, and *F. nucleatum* suspensions were diluted to 10^5 CFU/mL at the absorbance of 0.2 at OD_{600nm} [32]. The bacteria suspensions were treated with UCNPs@TiO_2 at 1 mM or 2 mM with or without the 980 nm irradiation at an intensity of 2.5 W cm^{-2} for 5 min in every hour (h). Upon 0, 1, 2, 4, 6, 8, 10 and 12 h incubation, 10 μL of the suspension was serially-diluted and inoculated on Columbia blood agar supplemented with 3 g/L beef extract powder, 10 g/L peptone, 5 g/L sodium chloride, 15 g/L agar and 5% sheep blood plates. After 48 h of anaerobic incubation at 37 °C, the number of viable bacteria colonies was counted. All measurements were performed in triplicates [32].

2.9. Single-species biofilm formation on human dentin

Freshly-extracted human molars were collected to prepare dentin samples as substrates for biofilm formation. Teeth collection was approved by Institutional Review Board of Jilin University, School of Dentistry (Ref. H20180067). After crown removal, square-shaped dentin samples with 5 × 5 mm and a thickness of about 1 mm were cut with a diamond saw. The dentin squares were grinded with 2400 grit SiC paper to standardize the samples. Each tooth slice was soaked in ethanol for 24 h and autoclaved at 160 °C for 1.5 h. To mimic the subgingival conditions, FBS was heat-inactivated to exclude complement-activity and used in a 25% concentration in saline. The dentin squares were immersed in the above solution at 37 °C overnight to pre-coat a serum pellicle on dentin [33].

Each bacteria species was used individually to form single-species biofilms following a previous study [32]. The serum pellicle-coated dentin squares were placed into a new 24-well plate. Each bacterial species was inoculated at a concentration of 10^8 CFU/mL in 1.5 mL medium in each well. The samples were treated with UCNPs@TiO_2 at a concentration of 1 mM and 2 mM upon 980 nm laser irradiation. Groups without laser irradiation served as control. The medium containing UCNPs@TiO_2 at different concentrations was refreshed every 24 h. After transferring to new 24-well plates, the dentin squares with adherent biofilms were treated with light irradiation in the same manner as the first day. The experiments following previous reports indicating that relatively mature biofilms could be formed in about four days [32].

For anti-biofilm evaluation, a commercial agent (TBO, Fotosan, CMS Dental A/S, Kopenhagen, Denmark) was included for comparison. According to the manufacturer, TBO-based treatment has antimicrobial (bacteria, virus, fungi) effects without risks or side-effects, and hence is an important adjunct to the scaling and root planing in the treatment of periodontitis. In addition to treating periodontitis, Fotosan is also used for the treatment of endodontic defections, gingivitis and other acute inflammatory conditions, including peri-implantitis and profound caries. In the present study, the TBO agent was prepared in the medium at a concentration of 0.1 mg/mL. The light source was a red light-emitting diode (LED) lamp with a wave length of 630 nm at an intensity of 2 W cm^{-2}, and TBO was used in its highest viscosity. This group is referred to as "Commercial aPDT control". The commercial aPDT control together with the aforementioned five groups were tested in the following experiments.

2.10. Live/dead staining

Each dentin square with 4-day biofilms was washed with cysteine peptone water (CPW) to rinse off the non-adherent bacteria. LIVE/DEAD BacLight Bacterial Viability Kits was used to examine the viability of the bacteria on the dentin slices following the manufacturer's instructions. The staining solution was mixed with 2.5 μM SYTO9 and 2.5 μM propidium iodide

to stain each sample for 15 min. Intact bacterial cells were stained with SYTO9 to emit a green fluorescence, whereas embrane-compromised bacterial cells were stained with propidium iodide to show a red fluorescence. The images of biofilms were collected with a CLSM (Olympus FV1000, Japan). Three dentin squares were tested for each group with each bacterial species, using a total of 54 dentin squares for live/dead staining. Five images were randomly captured for each sample, yielding 15 images for each group with each bacterial species.

2.11. *Colony-formation units counts*

For CFU testing, eighteen disks were made for each group, with six squares for each species. Dentin squares with 4-day biofilms were transferred into vials with 1 mL CPW, and the bacteria which were composed of biofilms were harvested by scraping and sonication/vortexing (IKA Lab Dancer, Germany). Columbia Blood Agar plates were used for CFU measurement. Biofilm suspensions were serially diluted, spread onto agar plates and incubated at 37 °C anaerobically for 72 h. Then, the number of growing colonies were counted and calculated CFU counts along with the dilution factor [32].

2.12. *Metabolic activity*

Eighteen disks were made for each group for the metabolic assay, with six squares for each bacterial species. The MTT assay is a colorimetric assay that is based on the transform from MTT into formazan crystals by living cells, which measures mitochondrial activity [34]. Each dentin square with 4-day biofilms was transferred to new 24-well plates with 0.4 mL of MTT dye (0.5 mg/mL MTT in PBS) in each well and incubated at 37 °C in 5% CO_2 for 1 h. The square was then transferred to new 24-well plates, and equal volume of DMSO was added to each well to solubilize the formazan crystals. The plates were sway gently on an incubated shaker (IS-RSDA, Incushaker, Crystal Technology & Industries Inc, USA) for 20 min at room temperature in the dark. After mixing well, 100 μL of the DMSO solution was transferred to a 96-well plate, and the absorbance at OD_{540nm} was measured via microplate reader (Bio-Tek). A higher absorbance value indicates a higher metabolic activity in the biofilm on the dentin squares.

2.13. *Statistical analysis*

Statistical analyses were performed by SPSS 19.0 software (SPSS, Chicago, IL, USA). All data were checked for normal distribution with the Kolmogorov-Smirnov test. One-way analyses of variance (ANOVA) were performed to detect the significant effects of the variables. Tukey's multiple comparison tests was used to compare the data at a pre-set alpha of 0.05.

3. Results

Fig. 1 showed representative TEM and HR-TEM images of the synthesized UCNPs and UCNPs@TiO_2. Typical TEM or HR-TEM images of β-$NaYF_4$: Yb^{3+},Tm^{3+} cores at low (Fig. 1A), medium (Fig. 1B) and high (Fig. 1C) magnifications showed that the nanoparticles were dispersed well with uniform size of (33.88 ± 0.79) nm in diameter and having a regular hexagonal shape. As shown in Fig. 1(D–F), TiO_2 could be seen on the surface of the UCNPs. Fig. 1F demonstrated the lattice fringes both on the core and the shell. The fringe spacing of 0.52 nm and 0.35 nm were exhibited corresponding to the 100 plane of β-$NaYF_4$ crystal and the 101 plane of anatase phase TiO_2, respectively. Fig. 1G showed the size distribution of UCNPs and UCNPs@TiO_2 by measuring the diameter on the TEM images. The TiO_2 coating on UCNPs increased the average diameter from 33.88 nm to 39.70 nm. The surface zeta potential of UCNPs@TiO_2 (Fig. 1H) showed a positive charge of approximately +12.4 mV.

Fig. 2A showed the powder XRD patterns of UCNPs and UCNPs@TiO_2. The position of the diffraction peaks from the UCNPs could be readily identified to the β-$NaYF_4$ structure according to the JCPDS standard card no. 16-0334. For UCNPs@TiO_2, besides the diffraction peaks of the β-$NaYF_4$ crystal, two main diffraction peaks of anatase phase TiO_2 (marked with stars) could also be observed according to the JCPDS standard card no. 21-1272. This further confirmed the combination of crystal TiO_2 and the β-$NaYF_4$:Yb^{3+},Tm^{3+} UCNPs. The UCL spectra of UCNPs and UCNPs@TiO_2 were shown in Fig. 2B. Triggered by the 980 nm laser, intense UV emission peaks centered at 348 nm and 362 nm which were assigned to the transitions of Tm^{3+} ions: $^1I_6 \rightarrow {}^3F_4$, and $^1D_2 \rightarrow {}^3H_6$, respectively. In addition, more intense blue UCL emission peaks centered at 450 nm and 480 nm due to the transitions of $^1D_2 \rightarrow {}^3F_4$ and $^1G_4 \rightarrow {}^3H_6$, respectively. Comparing the two upconversion spectra, after the modification of the TiO_2 shell, the ratio of UV/blue emissions sharply decreased relative to the unmodified UCNPs, indicating the energy transfer in the UV region from the UCNPs core to the TiO_2 shell. To further understand the photoluminescence and energy transfer process, Fig. 2C illustrated the principles of the upconversion mechanism and photocatalytic mechanism of TiO_2. The UCL decay curves of $^1I_6 \rightarrow {}^3F_4$ transitions of Tm^{3+} ions in UCNPs and UCNPs@TiO_2 under 980 nm light irradiation were shown in Fig. 2D. The decay time of UCNPs@TiO_2 remarkably diminished in comparison with UCNPs, for $^1I_6 \rightarrow {}^3F_4$ transitions due to the energy transfer to TiO_2. With increasing NIR irradiation time, the absorbance of DPBF was decreased at 410 nm, indicating the generation and release of the ROS as shown in Fig. 2E.

As shown in Fig. 3, both CCK-8 assay and cell staining with DAPI and FITC were performed to evaluate the dark-toxicity of UCNPs@TiO_2. The cell viability of L929 cells was over 95% at the concentration of 0.5 mM. When the concentration was 2 mM, the live cells still remained above 80%. Nevertheless, the numbers of cells alive decreased to below 50% at a concentration of 4 mM (Fig. 3A). Fig. 3(B–F) shows representative images of L929 cells at the presence of UCNPs@TiO_2 with different concentrations. The number of live L929 cells decreased dramatically at the concentration of 4 mM (Fig. 3F).

Fig. 4A showed a diagram of time-kill assay. Fig. 4B–D respectively plotted the time-kill curves for *S. sanguinis*, *P. gingivalis* and *F. nucleatum* at the first 12 h. The time-kill kinetics of different doses of UCNPs@TiO_2 without laser irradiation

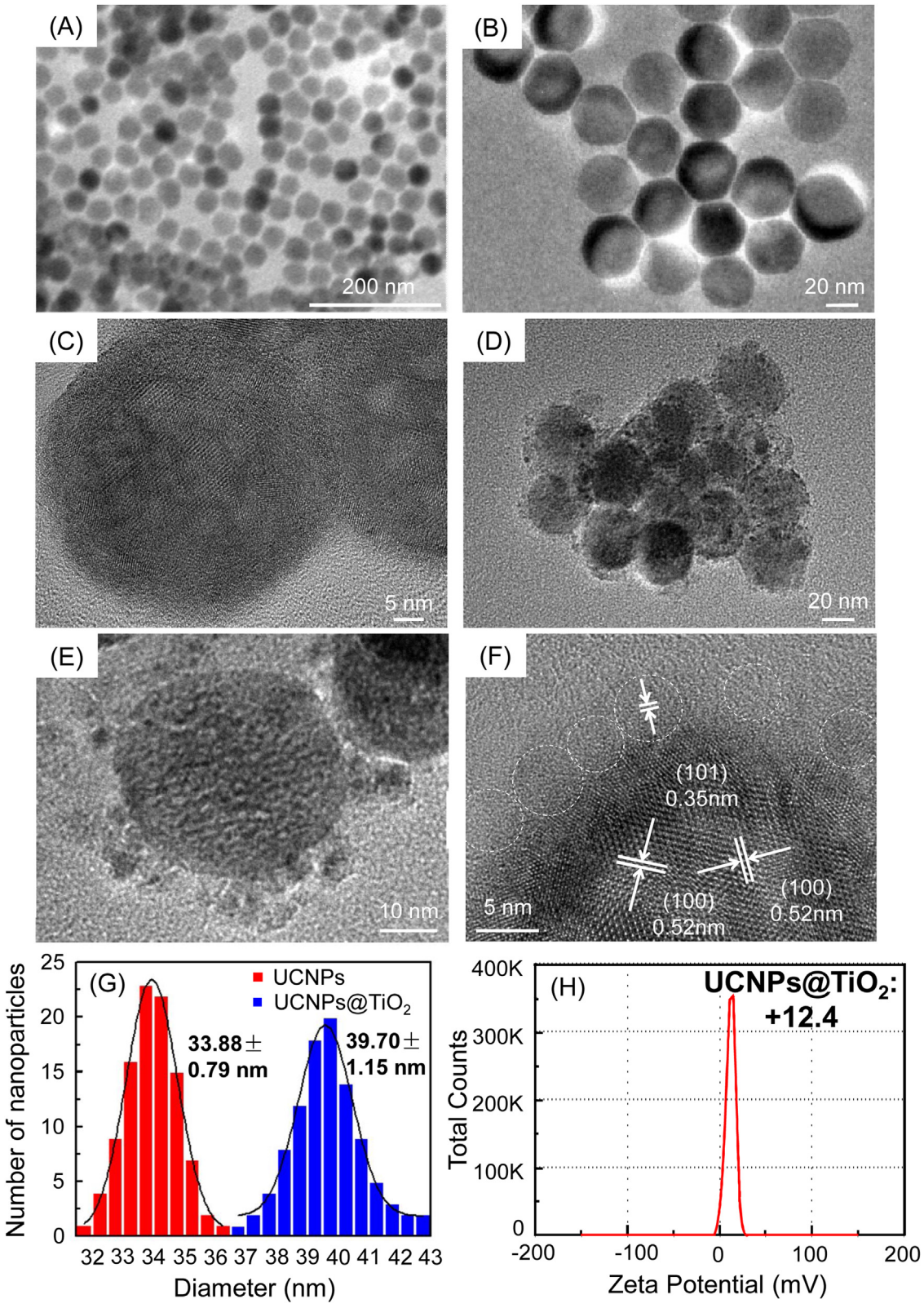

Fig. 1 – Morphology, size and zeta potential of UCNPs. (A–B) TEM images of UCNPs with different magnifications. (C) HR-TEM image of UCNPs. (D–E) TEM images of UCNPs@TiO_2 with different magnifications. (F) HR-TEM image of UCNPs@TiO_2. (G) Size distributions of UCNPs and UCNPs@TiO_2. (G) The zeta potential of UCNPs@TiO_2.

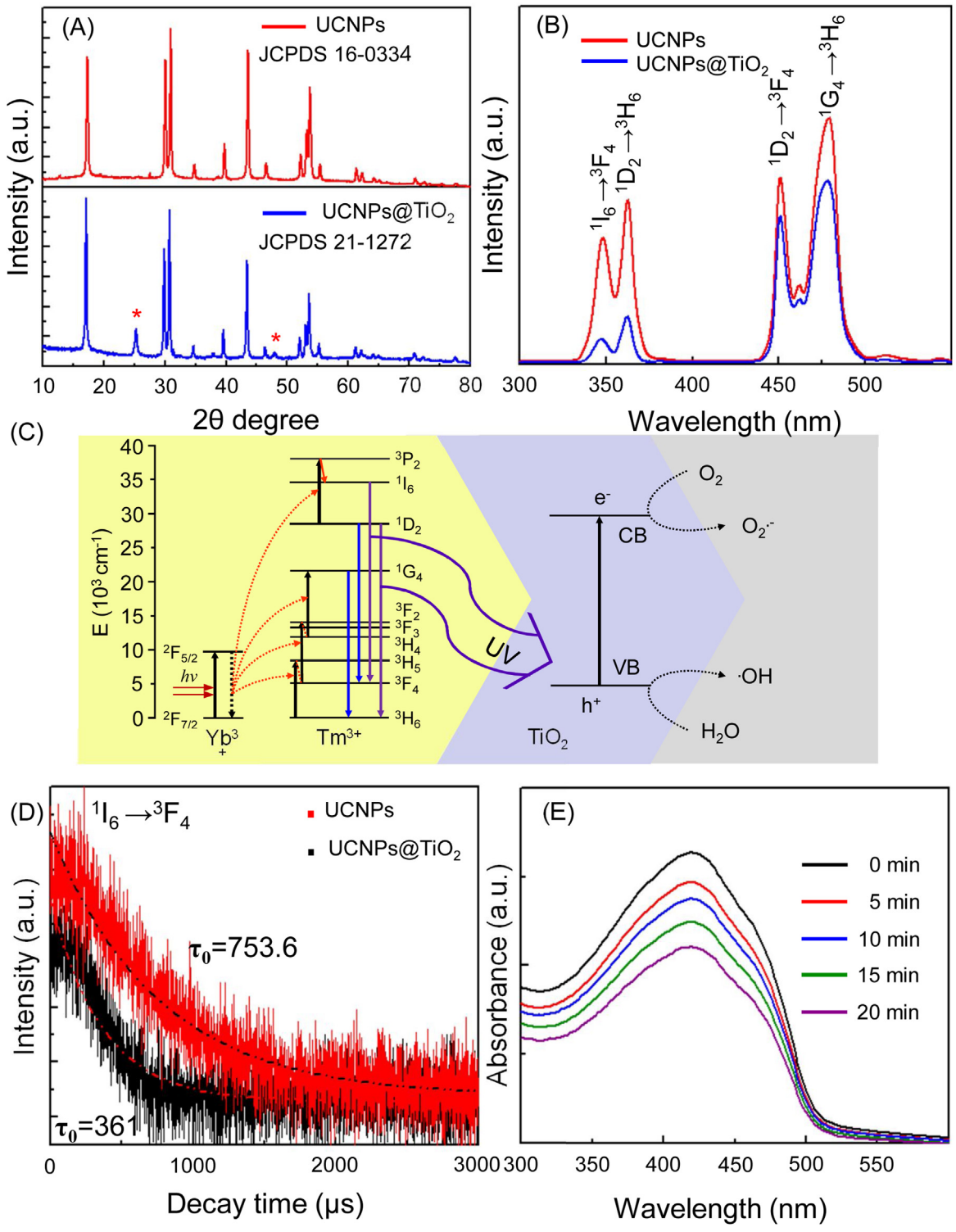

Fig. 2 – Characterization of UCNPs@TiO_2 and schematic image of energy transfer upconversion processes. (A) XRD patterns of UCNPs and UCNPs@TiO_2. Standard XRD patterns of JCPDS 16-0334 (β-$NaYF_4$) and JCPDS 21-1272 (TiO_2) were shown. "*" denoted anatase titania. (B) upconversion spectra of UCNPs and UCNPs@TiO_2 under 980 nm excitation. (C) Schematic illustration of energy transfer upconversion processes from $NaYF_4$: Yb^{3+},Tm^{3+} UCNPs to TiO_2 under 980 nm light excitation. (D) UCL decay curves of $^1I_6 \rightarrow {}^3F_4$ of Tm^{3+} transition in UCNPs and UCNPs@TiO_2 under 980 nm irradiation. (E) Absorbance of DPBF treated with UCNPs@TiO_2 under 980 nm irradiation for 20 min.

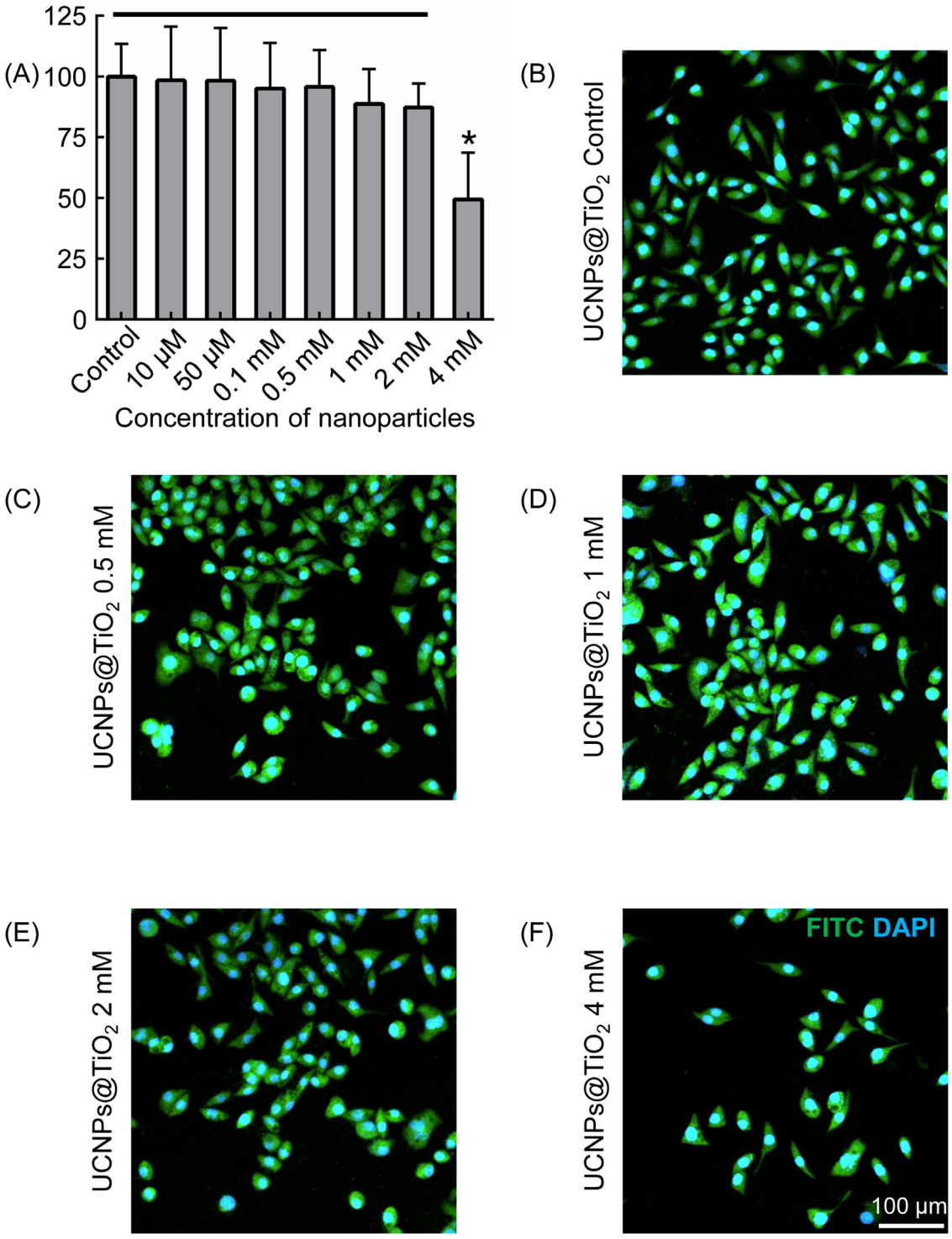

Fig. 3 – Dark toxicity of UCNPs@TiO_2. (A) L929 cell viability 24 h following in vitro in the dark cultured with UCNPs@TiO_2 at different concentrations. Solid line indicated that there was no significant difference between the groups. Asterisk indicated a significant difference ($p < 0.05$). (B–F) CLSM images of L929 cells incubated with UCNPs@TiO_2, showing green fluorescence indicating cytoplasm, Blue fluorescence indicates the nucleus. Scale bar: 100 μm. (For interpretation of the references to colour in this figure legend, the reader is referred to the web version of this article.)

resembled the dark control group, showing no antibacterial effects. In contrast, UCNPs@TiO_2 with the 980 nm laser irradiation killed all bacteria species at 12 h for 1 mM, and at 4 h for 2 mM.

Representative CLSM photographs of 4-day biofilms of *S. sanguinis*, *P. gingivalis* and *F. nucleatum* on dentin squares were shown in Fig. 5 for (A–C) Dark control, (D–F) commercial aPDT control, (G–I) Dark +1 mM UCNPs@TiO_2, (J–L) Dark +2 mM

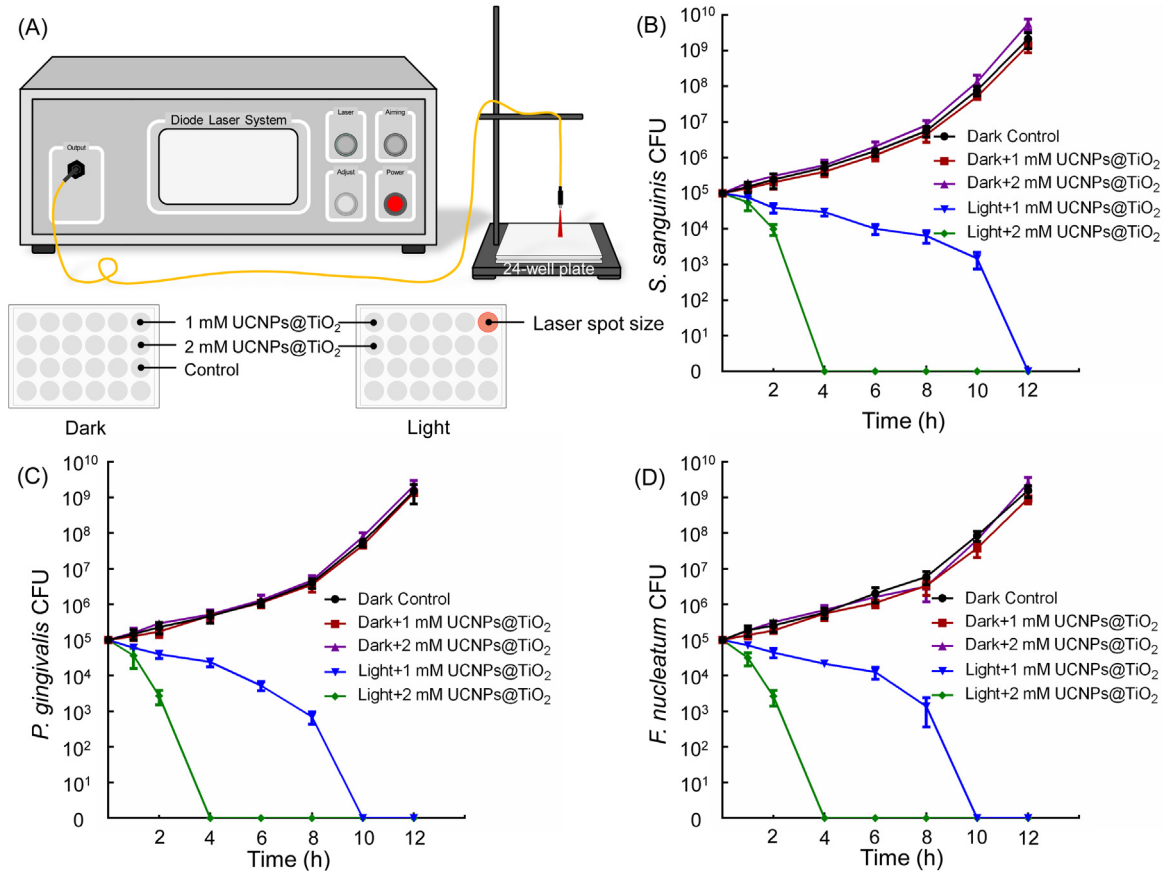

Fig. 4 – Time-kill assay of UCNPs@TiO_2 upon NIR irradiation against (B) *S. sanguinis* (C) *P. gingivalis* and (D) *F. nucleatum*. (A) Schematic illustration of the experiment process. Bacteria were cultured in medium containing UCNPs@TiO_2 at concentrations of 1 mM and 2 mM with or without NIR irradiation (980 nm, 2.5 W cm^{-2}, 5 min), as indicated for each curve in each plot. Note the log scale for the y-axis for colony-forming units (CFU). The surviving bacteria were plated at various time points as shown on the x-axis. All data points represented mean ± SD of three independent experiments.

UCNPs@TiO_2, (M–O) Light +1 mM UCNPs@TiO_2 and (P–R) Light +2 mM UCNPs@TiO_2. Live bacteria were stained green, and bacteria with compromised membranes were stained red. For all three species, three control groups were nearly fully covered by live bacteria. The commercial aPDT control showed less live bacteria. In contrast, the two UCNPs@TiO_2 groups with light irradiation had mainly red staining with compromised bacteria.

Fig. 6 plotted the CFU counts of 4-day biofilms on dentin squares (mean ± SD; n = 6). Dark control, Dark +1 mM UCNPs@TiO_2 and Dark +2 mM UCNPs@TiO_2 groups had similar CFU ($p > 0.1$). The commercial aPDT control decreased the biofilm CFU for all three species by 1–2 log. Upon NIR irradiation, the UCNPs@TiO_2 decreased the biofilm CFU for all three species by several orders of magnitude, compared to all dark groups ($p < 0.05$). The anti-biofilm properties of UCNPs@TiO_2 upon NIR irradiation showed a dose-dependent manner. The light +2 mM UCNPs@TiO_2 group had significantly lower CFU than the light +2 mM UCNPs@TiO_2 for *S. sanguinis* and *F. nucleatum* ($p < 0.05$). Using the light +2 mM UCNPs@TiO_2 as an example, the aPDT reduced the bacterial CFU differently for different bacterial species, some by approximate 3 log, others by more than 4 log. The CFU of *S. sanguinis*, *P. gingivalis* and *F. nucleatum* in the commercial aPDT control group were reduced to 11.2%, 1.03%, 2.43%, respectively, of the CFU in the Dark control group. While the CFU of *S. sanguinis*, *P. gingivalis* and *F. nucleatum* in the light +2 mM UCNPs@TiO_2 group were reduced to 0.021%, 0.003%, 0.005%, respectively, of the CFU in the Dark control group.

The MTT metabolic activity of 4-day biofilms on dentin squares was plotted in Fig. 7 (mean ± SD; n = 6). All three dark groups had similar MTT metabolic activity for all three species ($p > 0.1$). The commercial aPDT control group lowered the metabolic activity of biofilms of all three species ($p < 0.05$). The light +1 mM UCNPs@TiO_2 and the light +2 mM UCNPs@TiO_2 groups substantially reduced the metabolic activity of biofilms of all three bacterial species, compared with dark control and commercial aPDT control groups ($p < 0.05$).

4. Discussion

Although aPDT methods have recently achieved remarkable progress in the treatment of periodontitis, further improvement of the treatment of deep tissues is still needed [15]. Since UV and visible light is the main source of excitation for the most popular PSs, they face the disadvantages of shallow

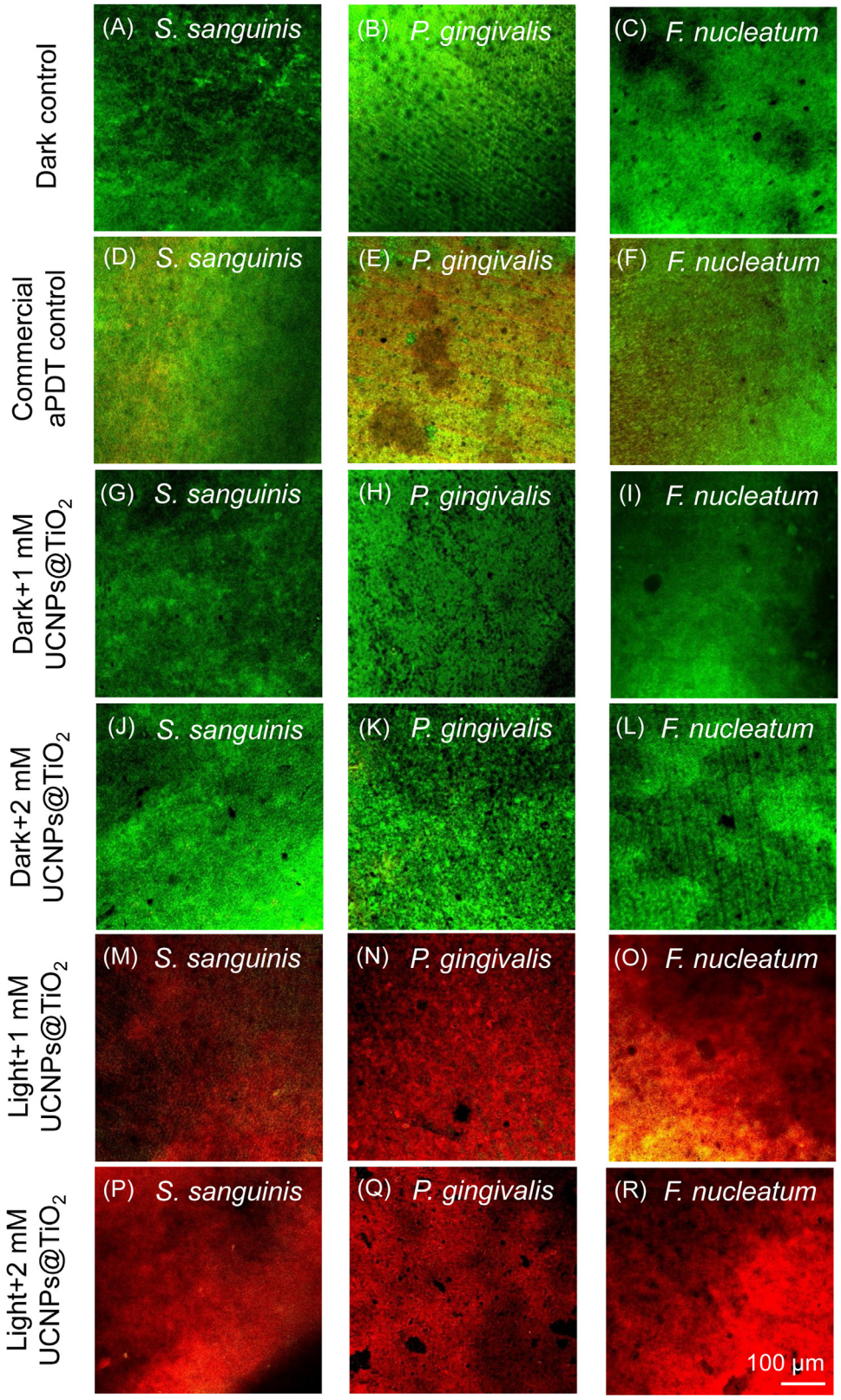

Fig. 5 – Representative live/dead images of 4-day biofilms on the dentin: *S. sanguinis* (left column), *P. gingivalis* (middle column) and *F. nucleatum* (right column) for (A–C) Dark control, (D–F) Commercial aPDT control, (G–I) Dark +1 mM UCNPs@TiO_2, (J–L) Dark +2 mM UCNPs@TiO_2, (M–O) Light + 1 m M UCNPs@TiO2 (980 nm, 2.5 W cm^{-2}, 5 min), and (P–R) Light +2 mM UCNPs@TiO_2 (980 nm, 2.5 W cm^{-2}, 5 min). Scale bar: 100 μm. Live bacteria were stained green, and dead bacteria were stained red. When live and dead bacteria were in close proximity or on the top of each other, the staining had yellow or orange colors. (For interpretation of the references to colour in this figure legend, the reader is referred to the web version of this article.)

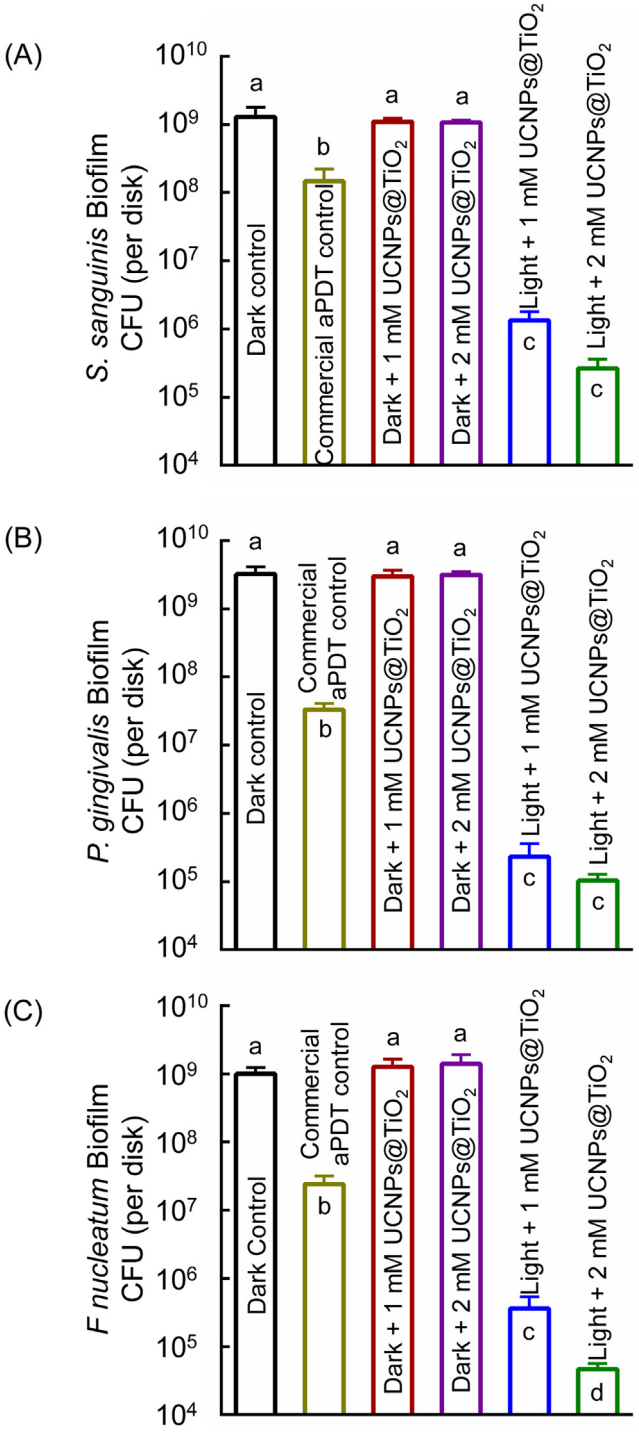

Fig. 6 – CFU counts of 4-day biofilms on dentin (mean ± SD; n = 6): (A) *S. sanguinis* (B) *P. gingivalis* and (C) *F. nucleatum* in different groups. Note the log scale for the y-axis. Dissimilar letters indicate values that were significantly different from each other ($p < 0.05$).

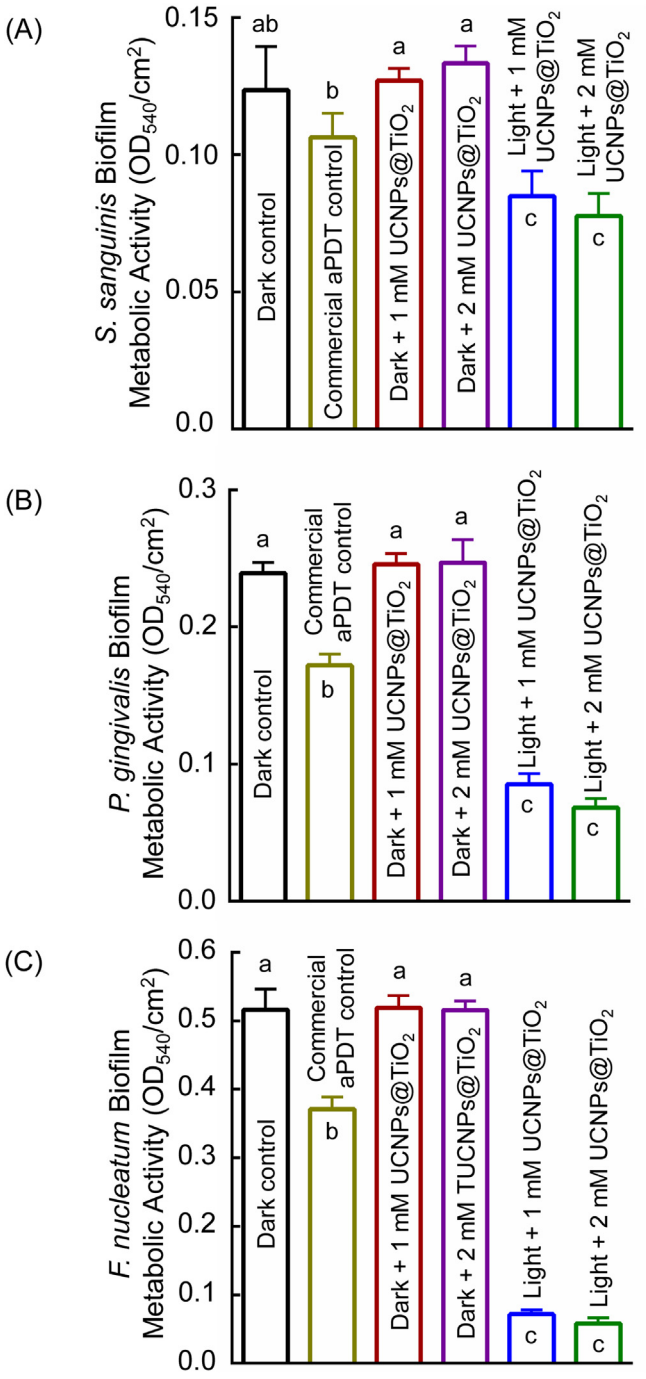

Fig. 7 – Metabolic activity of 4-day biofilms on dentin (mean ± SD; n = 6): (A) *S. sanguinis* (B) *P. gingivalis* and (C) *F. nucleatum* in different groups. Dissimilar letters indicate significantly different values ($p < 0.05$).

tissue penetration depth, and severe side effects when considering deep-level sterilization treatment applications [22]. Introducing NIR light with deeper tissue penetration is an important choice. As shown in the scheme 1, the most critical step is to convert NIR light into UV light, which is also a key innovation point in this sterilization work.

Rare earth-doped upconversion materials have anti-Stokes luminescence properties due to the sequential absorption of multiphoton by the ladder-like energy levels. Among the trivalent lanthanide ions, Tm^{3+} is the most important UCL centers which can convert NIR to UV. In addition, β-$NaYF_4$ is the most efficient UCL matrix material reported so far [35]. Therefore, in this work, β-$NaYF_4$:Yb^{3+},Tm^{3+} UCNPs were involved as the light conversion material and energy donor. The

core/shell-structure UCNPs@TiO_2 was further developed and the bactericidal effect against periodontitis-related pathogens excited by 980 nm laser was investigated for the first time. With the core/shell structure, the photocatalysis activity of TiO_2 could be induced by upconversion UV light, producing the electrons (e^-) in the conduction band (CB) and create a hole (h^+) in the valence band (VB). These electron-hole pairs migrate to the surfaces to induce in ROS generation (a schematic illustration is also demonstrated in Fig. 2C). Therefore, when the NIR-triggered aPDT is applied with deeper tissue penetration, it may become an effective method to solve the current bottleneck problem, which is also of utmost importance for clinical therapeutic applications in periodontitis. Note that all the hypotheses have been proven. The synthesized UCNPs@TiO_2 was uniform in size without noticeable cytotoxicity. The UCNPs@TiO_2 showed excellent performance in killing both planktonic bacteria and biofilms especially for Gram-negative bacterial species.

To identify the feasibility of NIR-triggering TiO_2, the UCL spectra were investigated. After coating a TiO_2 shell on the surface of UCNPs, both the blue and UV emission intensities decreased. Furthermore, upconverted UV light has experienced a much greater reduction than blue light emission, implying the energy transfer from UCNPs to TiO_2 at the UV region (Fig. 2B). This energy transfer process can be further explained by lifetime measurements. The transitions of the luminescent center of the rare earth include radiation transitions and non-radiative transitions. In this UCNPs@TiO_2 model, the energy transfer from the rare earth luminescence center to TiO_2 shell is a non-radiative transition. If the non-radiative transitions are enhanced, such as using resonance energy transfer or quenching, the fluorescence lifetime will be reduced due to the faster non-radiative transition rate. In this study, the UCL decay curves of $^1I_6 \rightarrow {}^3F_4$ transitions of Tm^{3+} ions in UCNPs and UCNPs@TiO_2 were investigated, which corresponds to the upconversion UV emission. Under the 980 nm light excitation, both UCL decay curves could be well-fitted to a single exponential function. However, compared to the UCNPs, the decay time for $^1I_6 \rightarrow {}^3F_4$ transition in UCNPs@TiO_2 was reduced by 52%. The decreasing of the fluorescence lifetime implied that the efficient energy migration between $NaYF_4$:Yb^{3+},Tm^{3+} and TiO_2 which belongs to a fluorescence resonance energy transfer (FRET) process. This energy migration contributed to the NIR-induced photocatalytic activity of TiO_2.

In this study, we only measured the ROS production in the first 20 min, since the radiation time would not last more than 20 min in clinical applications. In a previous study, the absorbance of DPBF was decreased by approximate 50% in 20 min [28]. However, the absorbance of DPBF was decreased by approximate 32.4% in 20 min upon NIR radiation in the present study. The yield of ROS production was not as much as those in previous study, which would probably decrease the antibacterial efficacy. First, the concentration of TiO_2 nanoparticles and DPBF probe in the previous study was 50-time higher than that in present study [28]. Second, when the NIR laser is used, only a very tiny light column can be used to achieve a relatively high excitation power density. However, as the DPBF probe is used to detect ROS, the ROS is generated only in a small excitation light column region. Rapid diffusion into the entire solution system happens quickly, which is equivalent to dilution of the ROS solution, that is why no significant absorption decline of probe can be observed. However, when applied to clinical treatment, that small point of stimulation is sufficient, because the area that needs treatment is relatively small. In addition, this concentrated NIR beam would be probably beneficial for clinical treatments. Since pathogenic factors such as dental calculus and plaque were relatively fixed and the inflammatory site was circumscribed, the area of the laser spot would be large enough to cover the periodontal lesion. Therefore, the ROS would be sufficient to combat pathogens in a narrow and deep periodontal pocket.

The UV spectrum ranged from 100 nm to 400 nm and its wavelengths could be subdivided into UVC (100–280 nm), UVB (280–315 nm) and UVA (315–400 nm). UV had strong bactericidal effects against oral bacteria such as *P. gingivalis*, *F. nucleatum*, *Enterococcus faecalis* (*E. faecalis*), and *S. sanguinis*. These bacterial strains were effectively eliminated with direct exposure to low doses of 254 nm UV light (2–7 mJ cm^{-2}) [36]. However, UV light radiation could increase the risk of DNA damage and UV-induced skin damage [25]. For short-term UV radiation, the DNA damages would be caused by exposure to $UV^{280\text{-}380}$ (1.6 kJ m^{-2}) and $UVB^{310\text{-}315}$ (1.5 kJ m^{-2}). In contrast, $UVA^{350\text{–}400}$ (150 kJ m^{-2}) did not lead to these DNA damages for both short-term and long-term exposures in a recent animal study [37]. In addition, bacteria suspensions alone with exposure to UV (365 nm) for 180 min showed no significant changes in live cell populations [38]. Therefore, $UVA^{350\text{–}400}$ was considered relatively safe for biological applications. In the present study, the UCNPs core were unlikely to be completely coated by TiO_2 without any photo-leakage. The UCNPs would upconvert NIR to a UV light at a wavelength of 365 nm, which belonged to the spectrum of UVA. Therefore, these upconverted UV by UCNPs would not lead to tissue damage.

The periodontitis-related pathogens showed a close relationship with the periodontal pocket depth. With increasing depth, the number of pathogens also increased [39]. Therefore, the depth and power of the light penetration was essential to achieving effective bactericidal activity. Low tissue penetration power limited the UV light from in vivo biological applications. In contrast, the NIR light could achieve the greatest tissue penetration [40]. In a previous study, the maximum width of the free gingiva was 1.42 mm (mean value: 0.96 ± 0.24 mm) and the maximum thickness of buccal alveolar bone was 3.01 mm (mean 0.85 ± 0.45 mm), via clinical and radiographic measurements [41]. Ng et al. measured the energy loss of NIR laser transmitted through alveolar bone and gingiva [42]. For each millimeter increase in the bone thickness, there was a decrease of 8.6 mW in transmission. For each millimeter of increase in the gingival thickness, there was a decrease of 5.3 mW in transmission [42]. In the present study, the intensity of the NIR irradiation was 2.5 W cm^{-2} for 5 min every day. For clinical applications, the decrease in transmission would be negligible and the frequency would be acceptable for patients. Therefore, it was feasible and effective for the NIR-triggered aPDT to treat periodontal diseases. In addition, the phototoxicity of the 980 nm NIR laser was not measured in the present study, since a previous study showed no significant cell toxicity under the radiation intensity of up to 6.1 W cm^{-2} for 30 min [28]. For antibacterial experiments,

both the irradiation intensity and the total radiation time in the present study were lower than the reported parameters, indicating that the 980 nm light had no phototoxicity.

Among all the known oral bacteria, streptococci were associated with the early colony and the subgingival plaque [5]. *S. sanguinis* is a pioneer bacterium colonizing on the surfaces of saliva-coated tooth which is of vital importance in the dental plague formation [5]. *S. sanguinis* is a pioneer bacterium colonizing on the surfaces of saliva-coated tooth which is of vital importance in the process of dental plague formation [5]. Extensive intrageneric co-aggregation and production of extracellular polysaccharides by streptococci play an important role in the early stage of biofilm formation [39]. Although previous studies indicated that *S. sanguinis* was a benign or even a beneficial bacterium for inhibiting periodontal pathogens [43], it was also considered as an important etiologic agent of infective endocarditis, particularly in people with predisposing cardiac valvular damage [44]. Because of the location of *S. sanguinis* in the oral cavity, introduction into the bloodstream was a hazard and could occur as a result of practices such as oral surgery [45]. Therefore, *S sanguinis* is a bacterium with a dual nature, having roles in both health and diseases [46]. Furthermore, from an immunological point of view, neutrophils are the predominant immune cells in periodontitis and produce ROS to clear the pathogens [46]. Indeed, several species, such as *P. gingivalis*, *F. nucleatum*, and oral streptococci, could scavenge and reduce the local level of neutrophil-derived ROS. This bacterial defense mechanism may prevent other biofilm organisms from the ROS damage [46]. Socransky et al. investigated 185 subgingival plaque samples and classified bacterial species into five major complexes [39]. The red complex showed the strongest relationship with clinical parameters such as pocket depth and bleeding on probing, and the orange complex was related to pocket depth. These two complexes were highly significant for diagnosis of periodontitis. *P. gingivalis* and *F. nucleatum* were the representative bacterial species of the red and orange complexes. *P. gingivalis*, the best characterized periodontal pathogen for disease development, could inhibit host defense functions in the gingival epithelium by regulating the expression of stress response genes, and could further impair the gingival tissues and cause alveolar resorption by inducing the production of inflammatory factors [47]. *F. nucleatum* was crucial in the initiation and the progression of periodontitis. *F. nucleatum* could eliminate the immune cell and contribute to the recruitment of other pathogens [48]. Furthermore, the colonization by *P. intermedia*, another periodontal pathogen, was always detected in the presence of *F. nucleatum* [48]. Therefore, in the present study, *S. sanguinis*, *P. gingivalis* and *F. nucleatum* were selected in the investigation of the antibacterial and anti-biofilm efficacy of the NIR-triggered UCNPs@TiO_2.

TiO_2 photocatalysis had favorable photocatalytic activity and strong effects on bacteria eradication [49–51]. TiO_2 could damage the proteins and lipids [49], and induce bacterial membrane rupture [50] and destroy the membrane fatty acids of bacteria [51]. A previous study indicated that TiO_2 nanoparticles upon UV radiation (365 nm) could generate the most amount of total ROS among all the seven tested metal oxides, with great antimicrobial efficacy next to CuO [52]. Recently, Wei et al. designed a multifunctional nanodevice UCNPs@TiO_2 with D-amino acids (D-Tyr) for aPDT, triggered by NIR irradiation [53]. NIR light-triggered and multifunctional UCNP-based aPDT systems were constructed to eradicate multiple resistant bacteria, bacterial biofilms, and fungal infection for clinical antimicrobial therapies [54–56]. However, there were no reports on the antibacterial effects of NIR-triggered UCNPs@TiO_2 on periodontitis-related pathogens, which were investigated in the present study for the first time.

The present study showed that UCNPs@TiO_2 could effectively kill all the tested bacteria. All the tested species of planktonic bacteria were eliminated in 12 h in a low dose (1 mM). Bacterial CFU was reduced by at least 3 log. The time-kill curves and CFU analysis indicated that there was a dose-dependent killing efficacy against microorganisms via UCNPs@TiO_2-based aPDT. On the other hand, with increasing irradiation time, the lower dose of UCNPs@TiO_2 also achieved excellent antibacterial effects. Oxidative damage caused by ROS was the main mechanism of antimicrobial effect via aPDT [16]. Among the various ROS, hydroxyl radical (·OH) played key roles in killing bacteria [57]. It acted on TiO_2 surface and diffused into the solution surrounding the photocatalyst, and degraded the non-direct-contact organic compounds [51]. A previous study developed a NIR-triggered UCNP@TiO_2-D-Try that could spatio-temporally release the free D-amino acids (D-Tyr) for biofilm dispersion and generated ROS against the bacteria [53]. Upon exposure to a 980 nm diode laser for 1.5 h (10 W cm^{-2}), the biofilm of *Bacillus subtilis* was disassembled with overnight incubation [53]. In the present study, even though the intensity of the NIR laser and the irradiation time were less than those in the previous study, excellent antibacterial effects against biofilms were still achieved. The advantage of a lower power NIR was that it decreased the risk of tissue thermal damage. The advantage of a short treatment time was that it minimized the patient's suffering. These advantages of the present study may have great significance for clinical treatments, which warrant further investigation.

Currently, although commercial PS such as methylene blue (MB) or Toluidine blue O (TBO) have been applied in clinical treatments for periodontal diseases, their inferior antibacterial effects and their drawback of gingiva staining have limited their applications. For example, a previous study reported that the synergism of light and MB-loaded cationic nanoparticles had a killing effect of only 85% on planktonic bacteria collected from patients with chronic periodontitis [58]. With exposure to the light, free MB, MB-loaded anionic, and cationic nanoparticles reduced the bacterial viability of biofilms by only 37%, 42%, and 48%, respectively [58]. TBO showed a similarly low antibacterial efficacy to MB. Using a combination of 0.33 mM TBO and LED irradiation at 60 mW cm^{-2} for 5 min, biofilms of *P. gingivalis* and *F. nucleatum* were, respectively, reduced by only 42% and 63%, compared to the non-PDT-treated control [59]. These low killing efficacies of the commercial agent-based aPDT against periodontal pathogens are not sufficient for clinical applications, since the remaining bacteria would quickly grow back. In the present study, the commercial aPDT group showed a 1–2 log reduction for all three species of biofilms, which is significantly inferior to the UCNPs@TiO_2 aPDT groups.

In the present study, the three species showed different degrees of difficulty to be killed by the NIR-triggered

UCNPs@TiO_2. The 4-day biofilm CFU results indicated that the extent of CFU reduction via NIR-triggered 2 mM UCNPs@TiO_2 was the greatest for Gram-negative species *P. gingivalis* and *F. nuleatum* (reduced to 0.003%-0.005% of dark control CFU), and the least for *S. sanguinis* (reduced to 0.021% of dark control CFU). The killing efficacy of UCNPs@TiO_2-based aPDT against biofilms of the three species was ranked to be: *S. sanguinis* < *F. nucleatum* = *P. gingivalis*. Conventional aPDT has greater efficacy against Gram-positive bacteria than Gram-negative bacteria [15]. Nevertheless, TiO_2-based aPDT exhibited a contrary effect, with more sensitivity against Gram-negative bacteria, which were predominantly colonized in subgingival biofilms during periodontitis. These results were also consistent with previous studies [38,60–62]. A previous study showed that the antimicrobial efficacy of anatase TiO_2 against *Escherichia coli* (*E. coli*, Gram-negative) was better than *Staphylococcus aureus* (Gram-positive) [60]. In addition, the bacteria susceptibility under photocatalytic action indicated the following sequence: *E. coli* > Gram-negative bacteria (other than *E. coli*) > *Enterococcus* species > Gram-positive bacteria [61]. Similarly, the susceptibility order of infectious agents under photocatalytic action was viruses > prions > Gram-negative bacteria > Gram-positive bacteria > yeasts > molds [62]. The first explanation was regarding the charge effects between the bacteria and PSs. Lipopolysaccharides (LPS) was one of the major components of outer membrane in Gram-negative bacteria [63]. LPS molecules with negative charge has a strong affinity for cations or cationic group. On the other hand, the generated ROS was more unstable and aggressive with a short life time and short diffusion range in aqueous media [64]. In the present study, the surface of UCNPs@TiO_2 exhibited a positive charge which would be conductive to its adherence to Gram-negative pathogens, which would facilitate the ROS to approach the bacteria and enhance the antibacterial efficacy. Secondly, TiO_2 could produce three types of ROS including hydroxyl radical, superoxide radical ($O_2^{\bullet -}$), and singlet oxygen ($^1O_2$). The majority of TiO_2 photocatalytic activity was attribute to hydroxyl radical [57]. Compared with Gram-negative species, Gram-positive bacteria required a greater number of hydroxyl radicals to achieve thorough bacterial inactivation, due to their thicker cell wall [60]. Huang et al. proposed that Gram-negative bacteria were possibly more susceptible to hydroxyl radical while Gram-positive bacteria were more susceptible to $^1O_2$ [65]. Therefore, TiO_2-based aPDT was more sensitive against Gram-negative bacteria than Gram-positive bacteria, consistent with the present study.

The in vivo effects of aPDT with UCNPs@TiO_2 under NIR irradiation were not investigated in the present study, due to the lack of an established and suitable animal model. Previous studies with animal models mainly focused on the reduction of bone resorption and alleviation of inflammation [66,67]. There has been no establishment of in vivo experimental model suitable for the investigation of aPDT antibacterial effects. In addition, the fiber-optic probe for humans is too large and inappropriate for use in small animals with induced periodontitis. Further studies are needed to investigate the aPDT effects of UCNPs@TiO_2 on the eradication of periodontal multispecies biofilms and the protection of the periodontium in a clinically-relevant animal model. In periodontitis treatments, besides intra-pocket administration, the UCNPs@TiO_2 could also be incorporated into dental composite and bonding agents to combat dental caries, or into root canal sealers to prevent secondary endodontic infections. The microenvironment of oral microbial communities is complex and diversified, and the infectious lesions are usually located in deep sites [68]. Therefore, the novel NIR-trigged UCNPs@TiO_2 method could be highly beneficial for a wide range of bacterial infections in the oral cavity, which requires further study.

5. Conclusions

This study synthesized core/shell-structured UCNPs@TiO_2 nanoparticles and investigated the NIR-triggered aPDT killing efficacy against periodontitis-related pathogens for the first time. UCNPs@TiO_2 possessed excellent biocompatibility with uniform size and positive charge on their surfaces. UCNPs@TiO_2 could convert the NIR light into UV light to trigger the TiO_2 which then produced ROS to kill the bacteria. UCNPs@TiO_2 showed a strong antimicrobial efficiency against periodontitis-related pathogens in both planktonic and biofilm phase upon NIR radiation. The time-kill curves showed that UCNPs@TiO_2 had great killing effects against all the tested bacteria, and eliminated all the bacteria in 4 h and 12 h at 1 mM and 2 mM, respectively. The application of 2 mM UCNPs@TiO_2 upon NIR radiation achieved the greatest reduction in biofilm growth and metabolic activity. The biofilm CFU was decreased by nearly 3–4 orders of magnitude for all three periodontitis-related pathogens. Therefore, UCNPs@TiO_2-based aPDT was highly effective in killing periodontal pathogens, combating periodontitis and protecting the periodontium. Novel NIR-triggered UCNPs@TiO_2 approach has exciting potential for treating a wide range of oral infectious diseases such as dental caries, endodontic infections, and peri-implantitis.

Acknowledgements

This work was supported by National Science Foundation of China 81570983 (YZ), 81400487 (LW), 61775080 (BD), International Cooperation of Science and Technology Jilin Province 20180414030GH (YZ), China Postdoctoral Science Foundation2015M581405, 2017T100213 (LW), 13th Five-Year Plan of the Science Foundation of Education Board of Jilin Province JJKH20180235KJ (LW), and University of Maryland School of Dentistry Seed Grant (HX).

REFERENCES

[1] Page RC, Kornman KS. The pathogenesis of human periodontitis: an introduction. Periodontol 2000 1997;14:9–11.
[2] Frencken JE, Sharma P, Stenhouse L, Green D, Laverty D, Dietrich T. Global epidemiology of dental caries and severe periodontitis-a comprehensive review. J Clin Periodontol 2017;44:S94–105.
[3] AlJehani YA. Risk factors of periodontal disease: review of the literature. Int J Dent 2014;2014:182513.

[4] Hajishengallis G. Periodontitis: from microbial immune subversion to systemic inflammation. Nat Rev Immunol 2015;15:30–44.
[5] Li J, Helmerhorst E, Leone CW, Troxler R, Yaskell T, Haffajee A, et al. Identification of early microbial colonizers in human dental biofilm. J Appl Microbiol 2004;97:1311–8.
[6] Feres M, Figueiredo LC, Soares GMS, Faveri M. Systemic antibiotics in the treatment of periodontitis. Periodontol 2000 2015;67:131–86.
[7] Jepsen S, Deschner J, Braun A, Schwarz F, Eberhard J. Calculus removal and the prevention of its formation. Periodontol 2000 2011;55:167–88.
[8] Krishna R, De Stefano JA. Ultrasonic vs. hand instrumentation in periodontal therapy: clinical outcomes. Periodontol 2000 2016;71:113–27.
[9] Meisel P, Kocher T. Photodynamic therapy for periodontal diseases: state of the art. J Photochem Photobiol B 2005;79:159–70.
[10] Jepsen K, Jepsen S. Antibiotics/antimicrobials: systemic and local administration in the therapy of mild to moderately advanced periodontitis. Periodontol 2000 2016;71:82–112.
[11] Rams TE, Degener JE, Van Winkelhoff AJ. Antibiotic resistance in human chronic periodontitis microbiota. J Periodontol 2014;85:160–9.
[12] Matesanz-Pérez P, García-Gargallo M, Figuero E, Bascones-Martínez A, Sanz M, Herrera D. A systematic review on the effects of local antimicrobials as adjuncts to subgingival debridement, compared with subgingival debridement alone, in the treatment of chronic periodontitis. J Clin Periodontol 2013;40:227–41.
[13] Takasaki AA, Aoki A, Mizutani K, Schwarz F, Sculean A, Wang CY, et al. Application of antimicrobial photodynamic therapy in periodontal and peri-implant diseases. Periodontol 2000 2009;51:109–40.
[14] Soukos NS, Goodson JM. Photodynamic therapy in the control of oral biofilms. Periodontol 2000 2011;55:143–66.
[15] Carrera E, Dias H, Corbi S, Marcantonio R, Bernardi A, Bagnato VS, et al. The application of antimicrobial photodynamic therapy (aPDT) in dentistry: a critical review. Laser Phys 2016;26:123001.
[16] Raghavendra M, Koregol A, Bhola S. Photodynamic therapy: a targeted therapy in periodontics. Aust Dent J 2009;54:102–9.
[17] Sharman WM, Allen CM, Van Lier JE. Photodynamic therapeutics: basic principles and clinical applications. Drug Discov Today 1999;4:507–17.
[18] Christodoulides N, Nikolidakis D, Chondros P, et al. Photodynamic therapy as an adjunct to non-surgical periodontal treatment: a randomized, controlled clinical trial. J Periodontol 2008;79:1638–44.
[19] Cadore UB, Reis MBL, Martins SHL, Invernici MdeM, Novaes Jr AB, Taba Jr M, et al. Multiple sessions of antimicrobial photodynamic therapy associated with surgical periodontal treatment in patients with chronic periodontitis. J Periodontol 2019;90:339–49.
[20] Chambrone L, Wang HL, Romanos GE. Antimicrobial photodynamic therapy for the treatment of periodontitis and peri-implantitis: an American Academy of Periodontology best evidence review. J Periodontol 2018;89:783–803.
[21] Shen S, Guo X, Wu L, Wang M, Wang X, Kong F, et al. Dual-core@shell-structured Fe_3O_4-$NaYF_4$@ TiO_2 nanocomposites as a magnetic targeting drug carrier for bioimaging and combined chemo-sonodynamic therapy. J Mater Chem B Mater Biol Med 2014;2:5775–84.
[22] Liu W, Su P, Chen S, Wang N, Wang J, Liu Y, et al. Webster, antibacterial and osteogenic stem cell differentiation properties of photoinduced TiO_2 nanoparticle-decorated TiO_2 nanotubes. Nanomedicine 2015;10:713–23.
[23] Cai Y, Strømme M, Melhus Å, Engqvist H, Welch K. Photocatalytic inactivation of biofilms on bioactive dental adhesives. J Biomed Mater Res B 2014;102:62–7.
[24] Shirai R, Miura T, Yoshida A, Yoshino F, Ito T, Yoshinari M, et al. Antimicrobial effect of titanium dioxide after ultraviolet irradiation against periodontal pathogen. Dent Mater J 2016;35:511–6.
[25] D'Orazio J, Jarrett S, Amaro-Ortiz A, Scott T. UV radiation and the skin. Int J Mol Sci 2013;14:12222–48.
[26] Chen G, Qiu H, Prasad PN, Chen X. Upconversion nanoparticles: design, nanochemistry, and applications in theranostics. Chem Rev 2014;114:5161–214.
[27] Lucky SS, Idris NM, Li Z, Huang K, Soo KC, Zhang Y. Titania coated upconversion nanoparticles for near-infrared light triggered photodynamic therapy. ACS Nano 2015;9:191–205.
[28] Hou Z, Zhang Y, Deng K, Chen Y, Li X, Deng X, et al. UV-emitting upconversion-based TiO_2 photosensitizing nanoplatform: near-infrared light mediated in vivo photodynamic therapy via mitochondria-involved apoptosis pathway. ACS Nano 2015;9:2584–99.
[29] Gomes A, Fernandes E, Lima JL. Fluorescence probes used for detection of reactive oxygen species. J Biochem Biophys Methods 2005;65:45–80.
[30] Gonçalves F, Zanetti AL, Zanetti RV, Martelli FS, Avila-Campos MJ, Tomazinho LF, et al. Effectiveness of 980-mm diode and 1064-nm extra-long-pulse neodymium-doped yttrium aluminum garnet lasers in implant disinfection. Photomed Laser Surg 2010;2:273–80.
[31] Wang L, Melo MA, Weir MD, Xie X, Reynolds MA, Xu HH. Novel bioactive nanocomposite for Class-V restorations to inhibit periodontitis-related pathogens. Dent Mater 2016;32:351–61.
[32] Sun X, Wang L, Lynch CD, Sun X, Li X, Qi M, et al. Nanoparticles having amphiphilic silane containing Chlorin e6 with strong anti-biofilm activity against periodontitis-related pathogens. J Dent 2019;81:70–84.
[33] Eick S, Kindblom C, Mizgalska D, Magdoń A, Jurczyk K, Sculean A, et al. Adhesion of *Porphyromonas gingivalis* and *Tannerella forsythia* to dentin and titanium with sandblasted and acid etched surface coated with serum and serum proteins — an *in vitro* study. Arch Oral Biol 2017;75:81–8.
[34] Van Meerloo J, Kaspers GJ, Cloos J. Cell sensitivity assays: the MTT assay. In: Cree IA, editor. Cancer cell culture methods and protocols. Humana Press Inc; 2011. p. 237–45.
[35] Li CX, Lin J. Rare earth fluoride nano-/microcrystals: synthesis, surface modification and application. J Mater Chem 2010;20:6831–47.
[36] Metzger Z, Dotan M, Better H, Abramovitz I. Sensitivity of oral bacteria to 254 nm ultraviolet light. Int Endod J 2007;40:120–7.
[37] Trucco LD, Mundra PA, Hogan K, Garcia-Martinez P, Viros A, Mandal AK, et al. Ultraviolet radiation-induced DNA damage is prognostic for outcome in melanoma. Nat Med 2019;25:221–4.
[38] Long M, Wang J, Zhuang H, Zhang Y, Wu H, Zhang J. Performance and mechanism of standard nano-TiO_2 (P-25) in photocatalytic disinfection of foodborne microorganisms — *Salmonella typhimurium* and *Listeria monocytogenes*. Food Control 2014;39:68–74.
[39] Socransky SS, Haffajee AD, Cugini MA, Smith C, Kent Jr RL. Microbial complexes in subgingival plaque. J Clin Periodontol 1998;25:134–44.
[40] Cui S, Yin D, Chen Y, Di Y, Chen H, Ma Y, et al. In vivo targeted deep-tissue photodynamic therapy based on near-infrared light triggered upconversion nanoconstruct. ACS Nano 2012;7:676–88.

[41] Stein JM, Lintel-Höping N, Hammächer C, Kasaj A, Tamm M, Hanisch O. The gingival biotype: measurement of soft and hard tissue dimensions — a radiographic morphometric study. J Clin Periodontol 2013;40:1132–9.
[42] Ng DY, Chan AK, Dalci O, Petocz P, Papadopoulou AK, Darendeliler MA. A pilot study of laser energy transmission through bone and gingiva. J Am Dent Assoc 2018;149:704–11.
[43] Lee SH. Antagonistic effect of peptidoglycan of *Streptococcus sanguinis* on lipopolysaccharide of major periodontal pathogens. J Microbiol 2015;53:553–60.
[44] Baker SP, Nulton TJ, Kitten T. Genomic, Phenotypic, and virulence analysis of *Streptococcus sanguinis* oral and infective-endocarditis isolates. Infect Immun 2019;87:e00703–18.
[45] Kinane DF, Riggio MP, Walker KF, et al. Bacteraemia following periodontal procedures. J Clin Periodontol 2005;32:708–13.
[46] Hirschfeld J, White PC, Milward MR, Cooper PR, Chapple lain LC. Modulation of neutrophil extracellular trap and reactive oxygen species release by periodontal bacteria. Infect Immun 2017;85, e00297-17.
[47] Darveau RP. Periodontitis: a polymicrobial disruption of host homeostasis. Nat Rev Microbiol 2010;8:481–90.
[48] Signat B, Roques C, Poulet P, Duffaut D. Role of *Fusobacterium nucleatum* in periodontal health and disease. Curr Issues Mol Biol 2011;13:25–36.
[49] Carré G, Hamon E, Ennahar S, Estner M, Lett MC, Horvatovich P, et al. TiO_2 photocatalysis damages lipids and proteins in *Escherichia coli*. Appl Environ Microbiol 2014;80:2573–81.
[50] Ranjan S, Ramalingam C. Titanium dioxide nanoparticles induce bacterial membrane rupture by reactive oxygen species generation. Environ Chem Lett 2016;14:487–94.
[51] Joost U, Juganson K, Visnapuu M, Mortimer M, Kahru A, Nõmmiste E, et al. Photocatalytic antibacterial activity of nano-TiO_2 (anatase)-based thin films: effects on *Escherichia coli* cells and fatty acids. J Photochem Photobiol B 2015;142:178–85.
[52] Li Y, Zhang W, Niu J, Chen Y. Mechanism of photogenerated reactive oxygen species and correlation with the antibacterial properties of engineered metal-oxide nanoparticles. ACS Nano 2012;6:5164–73.
[53] Wei W, Bing W, Ren J, Qu X. Near infrared-caged D-amino acids multifunctional assembly for simultaneously eradicating biofilms and bacteria. Chem Commun (Camb) 2015;51:12677–9.
[54] Yin M, Li Z, Zhou L, Dong K, Ren J, Qu X. A multifunctional upconverting nanoparticle incorporated polycationic hydrogel for near-infrared triggered and synergistic treatment of drug-resistant bacteria. Nanotechnology 2016;27:125601.
[55] Zhang Y, Huang P, Wang D, Chen J, Liu W, Hu P, et al. Near-infrared-triggered antibacterial and antifungal photodynamic therapy based on lanthanide-doped upconversion nanoparticles. Nanoscale 2018;10:15485–95.
[56] Dong K, Ju E, Gao N, Wang Z, Ren J, Qu X. Synergistic eradication of antibiotic-resistant bacteria based biofilms in vivo using a NIR-sensitive nanoplatform. Chem Commun (Camb) 2016;52:5312–5.
[57] Reddy PVL, Kavitha B, Reddy PAK, Kim KH. TiO_2-based photocatalytic disinfection of microbes in aqueous media: a review. Environ Res 2017;154:296–303.
[58] Klepac-Ceraj V, Patel N, Song X, et al. Photodynamic effects of methylene blue-loaded polymeric nanoparticles on dental plaque bacteria. Lasers Surg Med 2011;43:600–6.
[59] Park D, Choi EJ, Weon KY, et al. Non-invasive photodynamic therapy against-periodontitis-causing Bacteria. Sci Rep 2019;9:8248.
[60] Chung CJ, Lin HI, Chou CM, Hsieh PY, Hsiao CH, Shi ZY, et al. Inactivation of *Staphylococcus aureus* and *Escherichia coli* under various light sources on photocatalytic titanium dioxide thin film. Surf Coat Technol 2009;203:1081–5.
[61] Markowska-Szczupak A, Ulfig K, Morawski A. The application of titanium dioxide for deactivation of bioparticulates: an overview. Catal Today 2011;169:257–69.
[62] Bogdan J, Zarzyńska J, Pławińska-Czarnak J. Comparison of infectious agents susceptibility to photocatalytic effects of nanosized titanium and zinc oxides: a practical approach. Nanoscale Res Lett 2015;10:309.
[63] Malik Z, Ladan H, Nitzan Y. Photodynamic inactivation of Gram-negative bacteria: problems and possible solutions. J Photochem Photobiol B 1992;14:262–6.
[64] Redmond RW, Kochevar IE. Symposium-in-print: singlet oxygen invited review. Photochem Photobiol 2006;82:1178–86.
[65] Huang L, Xuan Y, Koide Y, Zhiyentayev T, Tanaka M, Hamblin MR. Type I and Type II mechanisms of antimicrobial photodynamic therapy: an in vitro study on gram-negative and gram-positive bacteria. Lasers Surg Med 2012;44:490–9.
[66] Camacho-Alonso F, Davia-Peña RS, Vilaplana-Vivo C, Tudela-Mulero MR, Merino JJ, Martinez-Beneyto Y. Synergistic effect of photodynamic therapy and alendronate on alveolar bone loss in rats with ligatureñinduced periodontitis. J Periodontal Res 2018;53:306–14.
[67] Zhang J, Liang H, Zheng Y, et al. Photodynamic therapy versus systemic antibiotic for the treatment of periodontitis in a rat model. J Periodontol 2019;90:798–807.
[68] Takahashi N. Microbial ecosystem in the oral cavity: metabolic diversity in an ecological niche and its relationship with oral diseases. Int Congr Ser 2005;1284:103–12.